separations

MDPI

Article

Natural Deep Eutectic Solvent-Based Ultrasound-Assisted Extraction of Flavonoids from *Fagopyrum tataricum* Bran

Zhou Xu [1,*], Xiaomei Da [2,3], Jipeng Qu [2] and Shiming Xiao [1]

[1] Panxi Crop Research and Utilization Key Laboratory of Sichuan Province, Xichang University, Xichang 615013, China
[2] College of Agricultural Sciences, Xichang University, Xichang 615013, China
[3] College of Life Science, Sichuan Agricultural University, Ya'an 625014, China
* Correspondence: xzhbiol@163.com or xzh@xcc.edu.cn

Abstract: In this study, eleven kinds of flavonoids were identified from *F. tataricum* bran (FTB) by UPLC-Q-TOF-MS, and HPLC-DAD analysis revealed that four compounds, including rutin, quercetin, kaempferol, and nicotiflorin, were the most significant components. Subsequently, natural deep eutectic solvent-based ultrasound-assisted extraction (NADES-UAE) was employed to extract flavonoids from FTB. Among the six kinds of NADES prepared, choline chloride–ethylene glycol (ChCl-EG) was identified as a promising candidate for extracting flavonoids due to its superior extraction performance. The extraction conditions were statistically investigated using response surface methodology conducted by Box-Behnken design (BBD). The optimal operational conditions were as follows: ultrasonic time 268 s, ultrasonic temperature 76 °C, and liquid–solid ratio 43 mL/g, which resulted in a high total flavonoid yield of 40.29 mg/g. Afterwards, the efficient extraction mechanism of NADES-UAE was comprehensively explored through FT-IR spectra, COSMO model, and microstructural analysis. In conclusion, NADES-UAE extraction is considered a green, efficient, and sustainable method for FTB flavonoids.

Keywords: *Fagopyrum tataricum* bran; natural deep eutectic solvent; ultrasound-assisted; UPLC-Q-TOF-MS; flavonoids; response surface methodology; COSMO model

Citation: Xu, Z.; Da, X.; Qu, J.; Xiao, S. Natural Deep Eutectic Solvent-Based Ultrasound-Assisted Extraction of Flavonoids from *Fagopyrum tataricum* Bran. *Separations* **2024**, *11*, 145. https://doi.org/10.3390/separations11050145

Academic Editor: Xiumei Li

Received: 9 April 2024
Revised: 2 May 2024
Accepted: 6 May 2024
Published: 8 May 2024

1. Introduction

Fagopyrum tararicum (tartary buckwheat) is an ancient dicotyledonous cultivated crop that originated in China and has been extensively planted in various countries, including China, India, Japan, Russia, and Korea [1]. *F. tararicum* is widely recognized as a nutritious and healthful food material, owing to its rich content of various physiologically active substances such as phytosterols, vitamins, carotenoids, fagopyritol, and flavonoids that are beneficial to health [2]. Notably, the flavonoids present in *F. tararicum* have garnered significant research attention in recent years owing to their abundant presence, unique composition, and remarkable bioactivities [3–5]. Numerous reports have demonstrated that the flavonoid compound content in *F. tararicum* bran (FTB) exceeds that of other milling fractions [5,6]. However, during the milling process of buckwheat grains, the flour is only used for food applications. The bran is usually discarded directly or used as animal feed, which fails to fully utilize the potential of this valuable resource. Thus, to minimize waste and increase the utilization rate of this underdeveloped material, it is essential to develop an efficient method for extracting flavonoid compounds from FTB.

Over the past few years, a novel category of green and designable solvents, known as natural deep eutectic solvents (NADES), have been extensively studied as potential replacements for conventional organic solvents in the extraction of natural products [7]. Typically, the components of NADES, including hydrogen bond donors (HBD) and hydrogen bond acceptors (HBA), are all derived from natural sources [8]. Thus, NADES has been recognized as promising new environmentally friendly solvents for the food,

feed, cosmetics, and pharmaceutical industries due to its offerings of several advantages, such as low operating costs, and sustainability, low or non-toxicity [9,10]. In addition, there is increasing evidence that NADES demonstrate strong extraction capabilities and biocompatibility when utilized for the extraction of bioactive compounds compared with traditional extraction reagents [11]. For example, research by Rashid et al. (2023) [12] demonstrated that NADES was more effective than 70% ethanol in extracting flavonoids and polyphenols from apple pomace. Jeong et al. (2015) [13] discovered that under the same conditions, the utilization of NADES as a solvent exhibited an extraction efficiency 1.85 times greater than that of methanol in the process of extracting anthocyanins from grape pomace.

It is important to note that, in addition to selecting a sustainable and environmentally friendly natural solvent as a green extraction solvent, the selection of extraction method is also crucial in the realm of green chemistry. Ultrasound-assisted extraction (UAE) is a widely used and environmentally friendly auxiliary method for extraction. It utilizes cavitation effects to disrupt the cell wall of plants, thereby facilitating the rapid and complete release of active components from plant cells into solvents [14]. This method is highly effective in extracting bioactive compounds from plant materials while minimizing environmental impact [15]. The NADES-UAE method ingeniously amalgamates the advantages of ultrasonic extraction and the use of NADES as a solvent, which has been widely utilized in extracting and separating various bioactive compounds from natural plants. However, as far as we are aware, there is a dearth of published literature regarding the utilization of the NADES-UAE method for the extraction of flavonoids from FTB.

Therefore, the objective of this study was to optimize the NADES-UAE extraction in order to achieve the maximum recovery of flavonoid content from FTB. The optimal conditions were achieved through the application of response surface methodology (RSM). And the efficient extraction mechanism of NADES-UAE was comprehensively explored through FT-IR spectra, COSMO model, and microstructural analysis.

2. Materials and Methods

2.1. Materials and Reagents

FTB (by-product of the processing of buckwheat flour) was acquired from Xichang Hangfei Buckwheat Technology Development Co., Ltd., Xichang, China. The sample was dried and ground into fine powder with a high-speed disintegrator, then passed through a 160-mesh sieve. Choline chloride (ChCl), betaine (Bet), ethylene glycol (EG), 1,2-propylene glycol (PG), and glycerol (Gly) were purchased from Shanghai Maclin Biochemical Technology Co., Ltd. (Shanghai, China). Chromatographic grade analytical standards rutin, quercetin, kaempferol, nicotiflorin, hyperoside, isoquercitrin, quercitrin, and apigenin were purchased from Chengdu Nakeli Biotechnology Co., Ltd. (Chengdu, China).

2.2. Identification of Flavonoid Compounds Using UPLC-Q-TOF-MS/MS

The flavonoid compounds in FTB were identified by UPLC-Q-TOF-MS/MS. The UPLC-Q-TOF-MS/MS system consisted of Waters ultra-performance liquid chromatography, an Xevo G2-XS quadrupole time of flight micro-mass spectrometer, electrospray ionization source, and BEH C18 column (2.1 mm × 100 mm, 1.7 μm) (Waters Corporation; Milford, MA, USA). The sample preparation for UPLC-Q-TOF-MS/MS analysis was as follows: 0.2 g of FTB powder was mixed with 2.0 mL of aqueous methanol (80%, *v*/*v*) and extracted for 30 min at 60 °C. Then, the clear extract solution was obtained through centrifuging (15,620× *g*, 5 min) and microporous membrane filtration (0.22 μm). The analysis conditions were set as follows: Injection volume 1 μL, column temperature 30 °C, mobile phase flow rate 0.3 mL/min, MS source temperature 120 °C, desolvation temperature 250 °C, capillary voltage 2.5 kV, mass scanning range 50 to 1500 (*m*/*z*). The mobile phase consisted of solvent A (0.1% formic acid water) and solvent B (acetonitrile), and the ratio of solvent A changed 95–90–80–60–20–0% with an analysis time of 0–5–8–14–18–20 min.

2.3. Quantification of Flavonoid Compounds Using HPLC

Flavonoid compounds rutin, nicotiflorin, quercetin, and kaempferol were quantitatively analyzed by Agilent 1260 high-performance liquid chromatography with a DAD detector and ZORBAX SB C18 column (4.6 mm × 150 mm, 5.0 μm) (Agilent, Santa Clara, CA, USA). The analysis conditions were set as follows: Injection volume 10 μL, column temperature 30 °C, DAD detection wavelengths 350 nm, mobile phase flow rate 1.0 mL/min. The mobile phase consisted of solvent A (0.1% formic acid water) and solvent B (acetonitrile), and the ratio of solvent A changed 90–90–60–20% with an analysis time of 0–5–20–30 min.

2.4. Preparation of NADES

Six kinds of NADES were prepared by magnetically stirring and heating methods. Briefly, the hydrogen bond acceptor (HBA), i.e., ChCl or Bet, was mixed either with the hydrogen bond donor (HBD), i.e., EG, PE, or Gly, at a molar ratio of 1:2. These solvents were continuously agitated in a water bath at 80 °C until a clear and uniform liquid was achieved. Subsequently, water (30%, *w*/*w*) was added to each prepared mixture to reduce viscosity.

2.5. Physico-Chemical Properties of NADES

Among physico-chemical properties: Viscosity, density and acidity were all analyzed. The viscosity was determined using a Ubbelohde viscometer, the density was conducted by measuring the mass of 10 mL liquid pipetted by glass pipet, and acidity was conducted using a pH meter.

2.6. Screening Extraction Solvent

In order to screen out the most efficient NADES for extraction, the six aforementioned NADES, along with methanol and ethanol, were utilized in the process. Briefly, 0.1 g of FTB powder was thoroughly mixed with 3.0 mL of extraction solvent (resulting in a liquid–solid ratio of 30 mL/g) in a crimp vial. The vial was exposed to 320 W of an ultrasonic bath for 120 s at a temperature of 40 °C. Then, the extracts were centrifuged at 15,620× *g* for 5 min, and clarified supernatant was collected and filtered with a 0.45 μm filter membrane before HPLC analysis.

2.7. Experimental Design of Extraction

2.7.1. Single Factor Experiment

Using ChCl-EG as the extraction solvent and ultrasonic bath power fixed at 320 W, a single-factor experiment was conducted to investigate the effects of different ultrasonic times (60, 180, 300, 420, and 540 s), different ultrasonic temperatures (40, 50, 60, 70, and 80 °C), and different liquid–solid ratios (10, 20, 30, 40, and 50 mL/g) on the extraction yield of flavonoids in FTB.

2.7.2. Response Surface Method

Based on the findings from single-factor experiments, the acceptable ratio ranges of ultrasonic time (X_1), ultrasonic temperature (X_2), and liquid–solid ratio (X_3) were obtained. Then, a three-levels-three-factors BBD design was utilized to determine the optimal extraction parameters by Design-Expert 9.0.0 software, and the experimental designs of each factor were presented in Table 1.

Table 1. Experimental designs and results of the response surface methodology.

Run	X_1	X_2	X_3	Extraction Yields (mg/g)				
	Ultrasonic Time (s)	Ultrasonic Temperature (°C)	Liquid–Solid Ratio (mL/g)	Rutin	Nicotiflorin	Quercetin	Kaemferol	Total Flavonoids
1	180	70	40	33.28	1.55	4.37	0.18	39.37
2	180	70	40	33.13	1.54	4.40	0.18	39.25
3	300	70	50	33.03	1.53	4.37	0.18	39.11
4	60	80	40	30.46	1.40	3.89	0.16	35.91
5	180	60	30	27.73	1.28	3.73	0.15	32.88
6	300	80	40	33.64	1.55	4.38	0.18	39.76
7	300	70	30	30.93	1.42	3.93	0.16	36.43
8	180	60	50	28.86	1.29	3.68	0.16	33.98
9	180	70	40	33.10	1.51	4.45	0.18	39.25
10	180	70	40	33.40	1.52	4.30	0.18	39.40
11	180	80	50	32.12	1.49	4.26	0.17	38.04
12	180	80	30	31.55	1.46	4.07	0.17	37.25
13	300	60	40	29.01	1.32	3.82	0.15	34.30
14	60	70	50	29.99	1.36	3.88	0.16	35.39
15	60	60	40	27.98	1.26	3.74	0.15	33.13
16	180	70	40	32.87	1.51	4.41	0.18	38.98
17	60	70	30	29.57	1.36	3.98	0.16	35.07

2.8. Fourier-Transform Infrared Spectroscopy

The Fourier-transform infrared (FT-IR) spectra of ChCl-EG and single components were determined with an infrared spectrophotometer (Nicolet iS20, Thermo Scientific, Waltham, MA, USA) with a 2 cm^{-1} resolution and analyzed in the range of 4000 to 400 cm^{-1}.

2.9. COSMOtherm Simulations

The structures of flavonoids and solution molecules were downloaded from PubChem, and the optimal molecular geometry and charge density of each molecule were calculated and optimized by density functional theory using the Dmol3 module in the Material Studio 2020 (Accelrys, San Diego, CA, USA). Then, the geometrically optimized structures were imported into COSMOThermX 18 (Dassault Systems, Paris, France), and the σ-surface and σ-profile of each molecule were calculated.

2.10. Scanning Electron Microscopy (SEM)

The microscopic morphology characterization was conducted according to previous studies [16]. Briefly, after extraction, all residual substances were sequentially washed three times with ethanol and water, followed by freeze-drying using a vacuum freeze dryer. The dried powder was coated with gold powder in a vacuum and imaged using a Zeiss Sigma 300 scanning electron microscope (Zeiss, Oberkochen, Germany).

2.11. Statistical Analysis

All assays were carried out in triplicate, and the results are expressed as the mean ± standard deviation (SD).

3. Results and Discussion

3.1. Identification of Flavonoid Compounds by UPLC-Q-TOF-MS

UPLC-Q-TOF-MS analysis has been broadly used to characterize flavonoids from various plant-based samples. In this study, flavonoid compounds from the FTB sample were subjected to non-targeted qualitative analysis by the LC-MS/MS method in negative ionization mode. An authentic standard, online database MASSBANK (https://massbank.jp/, accessed on 1 March 2024), and published literature were applied for the preliminary identification of the flavonoid compounds depending on their m/z readings and MS profiles in $[M - H]^-$ ionization mode. And compounds with a mass error of less than 5 ppm were

chosen as selection criteria for further m/z verification and MS/MS identification. The MS spectra of the flavonoids have been provided in Supplementary Material S1.

According to the retention times (Rt), major ion $[M-H]^-$, molecular formula, and MS/MS fragment ions, a total of 11 flavonoid compounds were identified (Table 2). Representatively, compound **3**, preliminarily identified as rutin, had a molecular ion at m/z 609 $[M-H]^-$ and a fragment ion at m/z 301 after the loss of a rhamnoside (146 Da) and a glucoside (162 Da) [17]. Compound **7** with a molecular ion at m/z $[M-H]^-$ 447 was identified as quercitrin, which first undergoes neutral depletion of $[M\text{-}H\text{-}146]^-$ from rhamnoside, yielding fragment ions of m/z 301, the quercetin ion. The quercetin ion proceeds undergoing Retro–Diels–Alder cleavage, producing fragment ions of m/z 179 and m/z 163 [18,19]. In addition, flavonoid molecular ions can be identified by the loss of neutral fragments (H_2O, CO, and CO_2). For example, apigenin (compound **9**), with a relative molecular mass of 270.24, readily loses H in the anion scan mode, and in the fragment ions m/z 225 $[M\text{-}H\text{-}CO_2]^-$, and m/z 151 $[M\text{-}H\text{-}CO_2\text{-}2CO\text{-}H_2O]^-$, in which losses of H_2O, CO, and CO_2 were detected [20,21].

Table 2. The flavonoid compounds identified in FTB using UHPLC-Q-TOF-MS/MS.

No.	Rt (min)	M.W.	Major Ion $[M-H]^-$ (m/z)	Molecular Formula	Fragment Ions MS/MS (m/z)	Identified Compounds
1	4.86	290.27	289.0689	$C_{15}H_{14}O_6$	245, 203, 179, 121, 109	Cianidanol
2	7.28	290.27	289.0689	$C_{15}H_{14}O_6$	245, 203, 179, 121, 109	Epicatechin
3	9.43	610.5	609.1259	$C_{27}H_{30}O_{16}$	301, 271, 255, 243	Rutin
4	9.56	464.38	463.0775	$C_{21}H_{20}O_{12}$	301, 300, 271, 255, 243, 227, 199, 151	Hyperoside
5	9.71	464.38	463.0731	$C_{21}H_{20}O_{12}$	301, 300, 271, 255, 243, 227, 199, 151	Isoquercitrin
6	10.20	594.52	593.1296	$C_{27}H_{30}O_{15}$	285, 255, 227	Nicotiflorin
7	10.52	448.38	447.0805	$C_{21}H_{20}O_{11}$	301, 271, 255, 243, 227, 179, 163, 151	Quercitrin
8	12.48	302.23	301.0315	$C_{15}H_{10}O_7$	179, 151, 121, 107, 93, 83	Quercetin
9	13.67	270.24	269.0428	$C_{15}H_{10}O_5$	225, 151, 149, 117, 107	Apigenin
10	13.88	286.24	285.0373	$C_{15}H_{10}O_6$	285	Kaempferol
11	14.21	316.26	315.0478	$C_{16}H_{12}O_7$	300, 271, 227, 163, 151, 148	Isorhamnetin

3.2. Physicochemical Properties of NADES

NADES is a typical kind of green solvent composed of HBA and HBD, which has currently garnered significant attention from both the academic and industrial sectors. Due to the fact that NADES is entirely composed of natural materials, such as sugars, organic acids, amino acids, and organic bases, they are considered much safer and more sustainable than traditional solvents [22]. As a practical and environmentally friendly alternative to ionic liquids, NADES has demonstrated excellent solvent properties for bioactive compounds, which makes it an ideal choice for a wide range of applications, including food engineering, personal care, and biological processes [23–25]. NADES consist of various HBAs and HBDs, each possessing distinct physicochemical properties such as pH values, polarities, density, and viscosities. These properties can significantly impact the dissolution of target compounds, thereby influencing the extraction yield. Therefore, assessing the physicochemical properties of the candidate NADES is essential.

As shown in Table 3, ChCl-PG exhibited the lowest density of 1082.94 mg/mL, while Bet-Gly demonstrated the highest density of 1181.16 mg/mL, and the densities of all six kinds of NADES were higher than water. Indeed, all DESs based on Bet displayed higher densities compared to their counterparts containing ChCl as HBA. Instead, with

respect to the HBD, the density decreased in the following sequence: Gly > EG > PG within the same families of NADES. As previously documented in the literature, intermolecular interactions are recognized as one of the primary factors that influence density. The greater the number of -OH functional groups present in the HBD, and consequently the increased potential for hydrogen bond formation, the higher the density of the system [26,27]. The viscosity of NADES represents the degree of resistance exhibited by a fluid, it represents another fundamental parameter that can be used to define their possible applicability as reaction or extraction media [28]. In this study, it is evident that Bet-based NADES exhibit significantly higher viscosity compared to ChCl-based NADES ($p < 0.05$). Among NADES with the same HBA, the viscosity follows the order: EG < PG < Gly for both ChCl and Bet-based solvents. The increased viscosities of Gly-containing NADES may be attributed to the presence of three hydroxyl groups and the higher molecular weight of glycerol [29,30]. In addition, the extraction efficiency can also be significantly influenced by the acid-base property of NADES, a chemical property that directly affects the solubility of a given solute in a solvent. Acidity test results showed that ChCl-Gly was the most acidic solvent with a pH of 4.38, while Bet-PG was the most alkaline solvent with a pH of 8.42. Furthermore, as with most of the NADES described in the literature, temperature and water have the ability to regulate the intermolecular cohesive forces in a NADES, which in turn contribute to their density, viscosity, and pH value [12,31,32].

Table 3. Composition and physicochemical properties of different NADES.

Label	HBA	HBD	Viscosity (mm^2/s)	Density (mg/mL)	pH
ChCl-EG	Choline chloride	ethylene glycol	9.32 ± 0.11^{f}	1105.43 ± 4.83^{d}	4.75 ± 0.01^{e}
ChCl-PG	Choline chloride	1,2-propylene glycol	15.11 ± 0.06^{d}	1082.94 ± 1.09^{f}	4.87 ± 0.01^{d}
ChCl-Gly	Choline chloride	glycerol	17.57 ± 0.12^{c}	1158.26 ± 0.90^{b}	4.38 ± 0.01^{f}
Bet-EG	Betaine	ethylene glycol	14.88 ± 0.06^{e}	1121.55 ± 2.31^{c}	8.24 ± 0.01^{b}
Bet-PG	Betaine	1,2-propylene glycol	24.59 ± 0.19^{b}	1095.25 ± 2.29^{e}	8.42 ± 0.01^{a}
Bet-Gly	Betaine	glycerol	33.65 ± 0.08^{a}	1181.16 ± 2.26^{a}	7.55 ± 0.02^{c}

Means with different letters within a row are significantly different ($p < 0.05$).

3.3. Screening the Optimal NADES

During the extraction process, the properties of solvents and solutes are closely interconnected, and their interactions have a significant impact on the rate of extraction. Given that the solvent structure of NADES plays a crucial role in determining the extraction rate and physicochemical properties of extracted flavonoids, it is essential to identify the most effective NADES for a specific application. In this experiment, the effects of six kinds of customized NADES on the extraction yield of FTB flavonoids were studied, and the results are shown in Figure 1. Meanwhile, methanol and ethanol, as two efficient solvents used in the extraction of natural products from biomass, have good extraction efficiency in previous studies and have been selected as references.

The resulting extracts were characterized using HPLC-DAD, and representative profiles can be found in Supplementary Material S2. All solvents exhibited similar profiles, with the peak attributed to rutin being significantly more abundant than others. And the other three distinct chromatographic peaks could be ascribed to nicotiflorin, quercetin, and kaempferol, respectively. These results are consistent with previous reports, which identified rutin, quercetin, kaempferol, and nicotiflorin as the primary flavonoid components in tartary buckwheat seeds [2,33]. Therefore, the four flavonoids mentioned above have been designated as target compounds in the subsequent extraction experiments, and the total extraction yield of the four flavonoids was used as the index to evaluate and optimize the extraction technology.

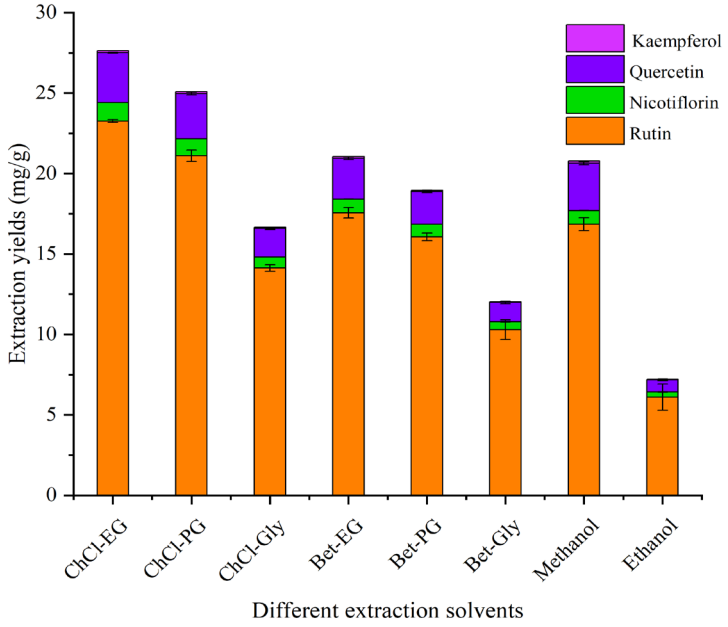

Figure 1. Effects of different solvents on the extraction yields of flavonoids in FTB.

As shown in Figure 1, the extraction yield on total flavonoids with ChCl-EG (27.63 mg/g) was significantly higher than that of other solvents, which was 1.33 folds of methanol and 3.84 folds of ethanol. Meanwhile, both ChCl-PG (25.09 mg/g) and Bet-EG (21.05 mg/g) also exhibited a higher extraction ratio than conventional extraction solvent methanol. It has been reported that the high affinity of hydrogen bonds enables NADES to effectively penetrate the cell wall structure, thereby promoting molecular interactions between NADES and plant cellulose chains and ultimately leading to a high extraction efficiency [34,35]. Furthermore, NADES has the capacity to donate and accept protons and electrons, thereby enabling the formation of hydrogen bonds between flavonoid compounds and NADES, consequently enhancing their solubility. [36,37]. Due to the excellent extraction efficiency of ChCl-EG, it was selected as the optimal NADES extraction solution for subsequent experiments.

3.4. Single Factor Experiment

3.4.1. Ultrasonic Time

Ultrasonic time is the most crucial parameter to be considered during the extraction process using the ultrasound assisted extraction technique. In this study, we investigated the yields of total flavonoids between 60 and 540 s of ultrasonic time while keeping other parameters constant (ultrasonic power 320 W, ultrasonic temperature 60 °C, and liquid–solid ratio 30 mL/g). As shown in Figure 2A, the flavonoids extraction yield increased with time and reached its maximum at 180 s, with a value of 32.49 mg/g. Subsequently, the extraction yield decreased as the ultrasonic time continued to increase. In general, prolonging the extraction duration can enhance the adequate dissolution of flavonoids in solvents. However, extended exposure to ultrasound may lead to structural defects in the flavonoids in the extracts. Hence, prolonged ultrasonic extraction is not recommended for labile flavonoids. This also confirms that ultrasound has the ability to dissolve compounds in plant cell walls within a relatively short period of time. Similar behavior was observed in the study about ultrasound-assisted natural deep eutectic solvent extraction of flavonoids in *Ampelopsis grossedentata* leaves [38]. Therefore, the ultrasonic time of 180 s was chosen for the follow-up experiment.

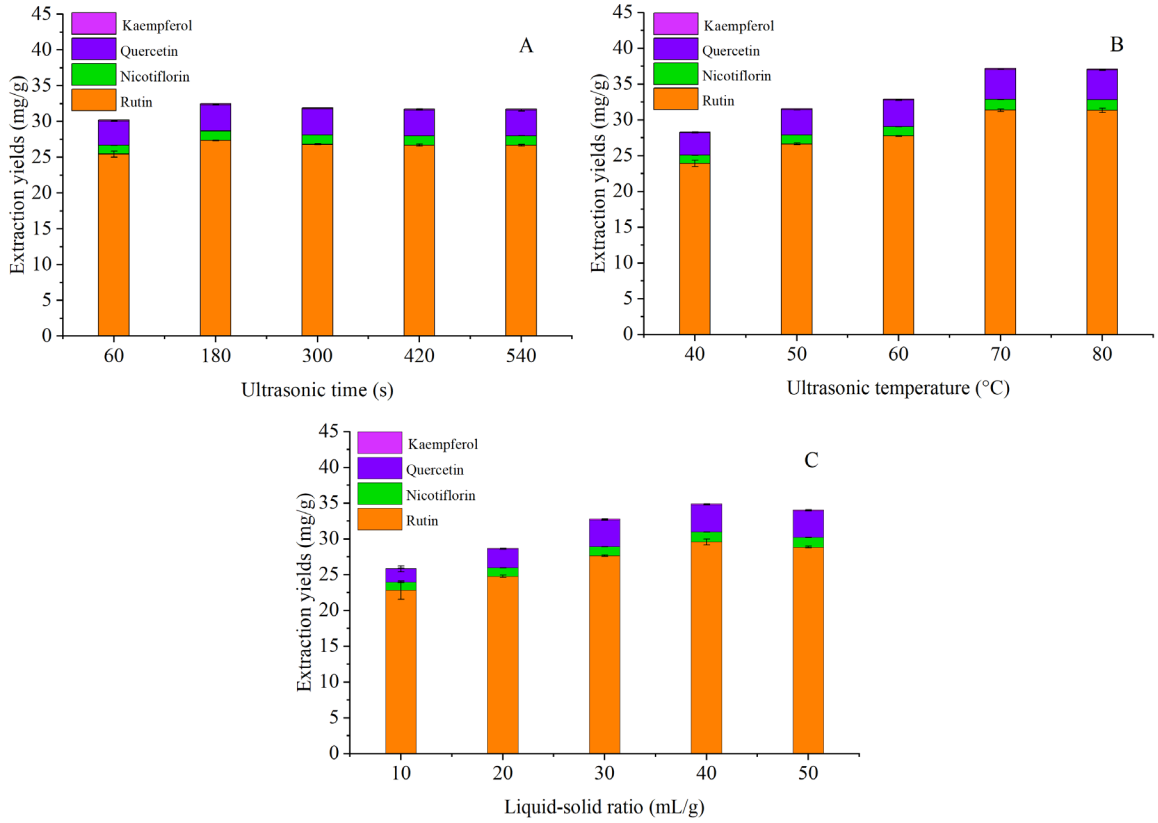

Figure 2. Effects of ultrasonic time (**A**), ultrasonic temperature (**B**), and liquid–solid ratio (**C**) on the extraction yields of flavonoids in FTB.

3.4.2. Ultrasonic Temperature

The selection of an appropriate extraction temperature is critical for the efficient recovery of flavonoids due to its impact on the interaction between flavonoids and protein/cellulose, as well as on the viscosity of the NADES [39]. In this study, the effect of ultrasonic temperature on the extraction efficiency of flavonoids was experimented with by differing the processing temperature from 40 to 80 °C while keeping other parameters constant (ultrasonic power 320 W, ultrasonic time 180 s, and liquid–solid ratio 30 mL/g), and the result is exhibited in Figure 2B. The ultrasonic temperature had an obvious effect on flavonoid yields. As the temperature increased, the extraction yield of flavonoids showed an increase and reached its maximum at 70 °C. Increasing the temperature could reduce the viscosity of NADES and increase the mass transfer rate [40]. Meanwhile, in the process of ultrasonic-assisted extraction, both the thermal effect and the cavitation effect play a significant role. An increase in temperature can enhance the cavitation effect, thereby improving the extraction efficiency to some extent. However, as the temperature continues to rise, the intensity of the cavitation effect will decrease [12,41]. In addition, flavonoids are always thermosensitive and might decompose when exposed to excessive temperatures [42]. Therefore, an extraction temperature of 70 °C was selected for the follow-up experiment.

3.4.3. Liquid–Solid Ratio

The liquid–solid ratio is a key parameter that significantly impacts the capital cost of extraction plants from a process profitability perspective. In addition, the mass transfer at the solid–liquid interface varies depending on the percentage of solids and the quantity of solvent [12]. Therefore, it is of significance to inspect the optimal liquid–solid ratio. In this study, the effect of liquid–solid ratio on the extraction efficiency of flavonoids was experimented with while keeping other parameters constant (ultrasonic power 320 W,

ultrasonic time 180 s, and ultrasonic temperature 60 °C), and the result is exhibited in Figure 2C. With increasing liquid–solid ratios, the flavonoids extraction efficiency first increased and then decreased, and when the liquid–solid ratio was 40 mL/g, the flavonoids extraction efficiency was the highest (34.94 mg/g). This phenomenon may be attributed to the increased contact area between the solute and solvent, which reduced the density of the mixture and increased the speed of ultrasonic propagation, thereby improving the dissolution rate [43]. Moreover, by increasing the liquid–solid ratio, flavonoid extraction efficiency shows a decreasing trend. This might be caused by tiny bubbles formed in high liquid–solid ratio more easily, that hindered the contact between flavonoids and the solvent, as well as affected the propagation of ultrasound, thereby reducing the dissolution efficiency [35]. Therefore, the liquid–solid ratio of 40 mL/g was selected for the follow-up experiment.

3.5. RMS-BBD Model Fitting and Response Surface Analysis

3.5.1. Predicted Model and Statistical Analysis

Based on the analysis of single-factor experiments, the independent variables, including ultrasonic time, ultrasonic temperature, and liquid–solid ratio, were used for further optimization of flavonoids extraction by Box–Behnken design (BBD). A total of 17 experimental runs with different combinations of the investigated variables were performed randomly, and the results are presented in Table 1. Through the application of multiple regression analysis to the experimental data, the relationship between the response variable and the test variables was modeled using the following second-order polynomial equation:

$$Y = 39.25 + 1.26X_1 + 2.08X_2 + 0.61X_3 + 0.67X_1X_2 + 0.59X_1X_3 - 0.077X_2X_3 - 1.26{X_1}^2 - 2.22{X_2}^2 - 1.49{X_3}^2 \quad (1)$$

where Y represents the extraction yield of total flavonoids (mg/g); X_1 denotes the ultrasonic time (s), X_2 denotes the ultrasonic temperature, and X_3 denotes the liquid–solid ratio, respectively.

The statistical significance of the regression equation was evaluated using the *F*-test and *p*-value and the ANOVA for the response surface quadratic polynomial model, as summarized in Table 4. The model *F*-value was 273.25 and *p*-value was less than 0.0001, which implied the regression equation was ideal and the model was highly statistically significant. Meanwhile, the lack of fit *F*-value was 1.93 and the associated *p*-value was 0.2664, which indicated that the lack of fit was not significant. The experiment values agreed with the predicted values excellently. The high values of determination coefficient (R^2 = 0.9972) and adjusted determination coefficient (*Adj* R^2 = 0.9935) indicated a satisfactory correlation between the experimental results and the predictive values predicted by this equation. The *CV* value of 0.53 indicated that the accuracy and general availability of the polynomial model were adequate. Additionally, the linear terms (X_1, X_2, and X_3), the interaction terms (X_1X_2 and X_1X_3), and the quadratic terms (${X_1}^2$, ${X_2}^2$, and ${X_3}^2$) were significant ($p < 0.05$) on extraction yield.

Table 4. ANOVA table for the response surface quadratic model.

Source	Sum of Squares	df	Mean Square	*F*-Value	*p*-Value
Model	94.43	9	10.49	273.25	<0.0001 **
X_1	12.75	1	12.75	332.09	<0.0001 **
X_2	34.74	1	34.74	904.67	<0.0001 **
X_3	2.99	1	2.99	77.85	<0.0001 **
X_1X_2	1.80	1	1.80	46.76	0.0002 **
X_1X_3	1.39	1	1.39	36.26	0.0005 **
X_2X_3	0.02	1	0.02	0.63	0.4549 ^{ns}
${X_1}^2$	6.64	1	6.64	173.06	<0.0001 **
${X_2}^2$	20.73	1	20.73	539.84	<0.0001 **

Table 4. *Cont.*

Source	Sum of Squares	df	Mean Square	*F*-Value	*p*-Value
X_3^2	9.39	1	9.39	244.68	<0.0001 **
Residual	0.27	7	0.04		
Lack of fit	0.16	3	0.05	1.93	0.2664 ^{ns}
Pure error	0.11	4	0.03		
Cor total	94.70	16			
R^2 = 0.9972	*Adj* R^2 = 0.9935	*CV* = 0.53			

** Very significant, $p < 0.01$; ^{ns} non-significant, $p > 0.05$.

3.5.2. Analysis of the Response Surface

In order to visually interpret the individual and interactive effect of extraction process parameters on flavonoids extraction yield, three-dimensional (3D) response surface and two-dimensional (2D) contour plots were plotted using Design-Expert 9.0.0 software (Figure 3). As shown in Figure 3A,B, when the liquid–solid ratio was fixed at 40 mL/g, the extraction yield of flavonoids increased evidently with increasing ultrasonic time from 60 to 258.43 s, but beyond 258.43 s, the extraction yield of flavonoids increased slowly as the ultrasonic time ascended. The extraction yield of flavonoids increased evidently with an increase in ultrasonic temperature from 60 to 75.69 °C, but beyond 75.69 °C, the yield of flavonoids increased slowly as the temperature ascended. Figure 3C,D shows the effects of ultrasonic time and liquid–solid ratio on the flavonoids extraction yield while the ultrasonic temperature was fixed at 70 °C. At an ultrasonic time of 249.25 s and a liquid–solid ratio of 43.18 mg/L, a maximum flavonoid extraction yield was obtained. Figure 3E,F shows the effects of ultrasonic temperature and liquid–solid ratio on the yield of flavonoids when ultrasonic time was fixed at 180 s. The extraction yield increased with an increase in the ultrasonic temperature and liquid–solid ratio from 60 to 74.60 °C and 30 to 41.91 mL/g, respectively. However, it decreased when the ultrasonic temperature and liquid–solid ratio were over 74.60 °C and 41.91 mL/g, respectively.

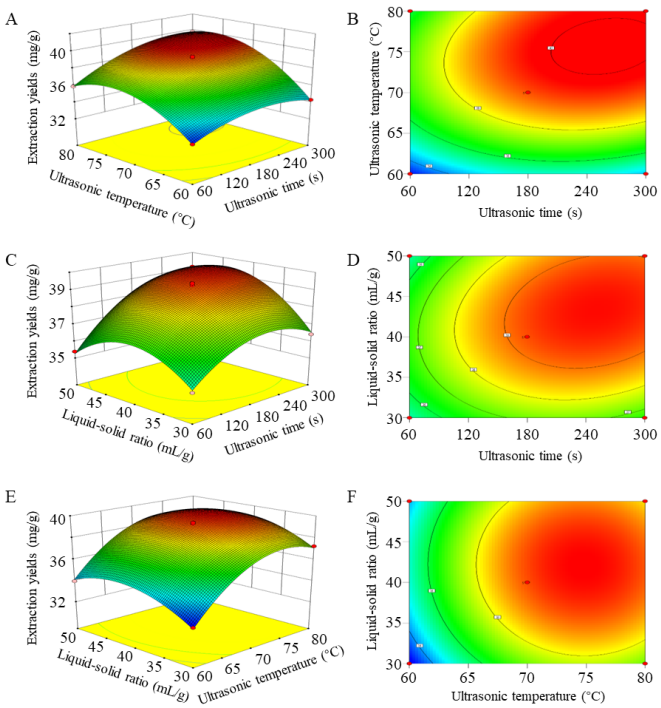

Figure 3. Response surface plots (**A**,**C**,**E**) and contour plots (**B**,**D**,**F**) of variable parameters, including ultrasonic time (X_1), ultrasonic temperature (X_2), and liquid–solid ratio (X_3), on the extraction yields of flavonoids in FTB.

3.5.3. Verification of Predictive Model

According to the RSM results, the optimal extraction conditions were ultrasonic time 268.12 s, ultrasonic temperature 75.74 °C, and liquid–solid ratio 43.35 mL/g, respectively. Under these conditions, the maximum predicted yield of FTB flavonoids was 40.41 mg/g. Due to operational limitations in the lab, the actual extractions were slightly modified: Ultrasonic time of 268 s, ultrasonic temperature of 76 °C, and liquid–solid ratio of 43 mL/g. Five verification experiments were conducted to validate the adequacy of the model equation, and the actual extraction yield was found to be 40.29 mg/g. No significant difference ($p > 0.05$) was observed between the actual experimental and predicted values, indicating that the model was accurate and suitable for extracting FTB flavonoids.

3.6. FT-IR Spectra of ChCl-EG and Single Component

In order to understand the hydrogen bond interactions between ChCl and EG, an FT-IR spectrum experiment was conducted, and the results are shown in Figure 4. In the IR spectrum of ChCl, the stretching vibration peak at 3249 cm^{-1} was assigned to the -OH stretching, and the sharp peaks at 3019 cm^{-1} belonged to the stretching vibration peak of -CH [39]. Meanwhile, a vibration band of the alkyl group was presented at 1485 cm^{-1}, which showed the characteristic of ChCl [44]. In the IR spectrum of EG, the broad 3400–3200 cm^{-1} belonged to the stretching vibration peak of -OH, the peaks at 2938 cm^{-1} and 2874 cm^{-1} belonged to stretching vibration of -CH_2, the peaks from 1600 to 1200 cm^{-1} assigned to the -CH_2- flexural vibration, and peaks around 1050 cm^{-1} belonged to stretching vibration of -C-O-. In the IR spectrum of ChCl-EG, the -OH stretching frequency shifted to a higher frequency of 3300 cm^{-1} compared with ChCl (3249 cm^{-1}) and EG (3289 cm^{-1}), which indicated that ChCl and EG formed new intermolecular hydrogen bonds as a result of intramolecular associations among the components [16]. Meanwhile, by comparing the shifting of the -OH functional groups in ChCl, EG, and pure ChCl-EG, it can be noticed that the band between 3000 and 3600 cm^{-1} in ChCl-EG had a tendency to be broader and wider, which also indicated the formation of hydrogen bonds during the preparation of the ChCl-EG [44]. From the spectroscopy data, it can also be inferred that the main characteristic functional groups of the monomeric compounds still coexisted after the formation of ChCl-EG, which was consistent with the conclusion of Zhang et al. and Hayyan et al. [11,45]. Finally, compared with ChCl-EG, the spectrum of ChCl-EG with 30% water showed little change, indicating that the addition of water did not disrupt the hydrogen bonding between ChCl and EG.

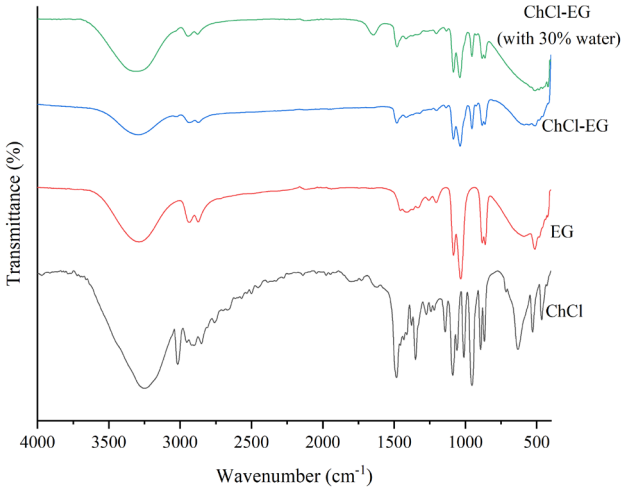

Figure 4. FT-IR spectra of ChCl-EG and its pure components (ChCl and EG).

3.7. Theoretical Support with COSMO Model Analysis

Previous research indicated that the COSMO model can be utilized to predict the affinity between solutes and solvents as well as reflect the charges in the molecular configuration. This predictive capability enables researchers to estimate solvent solubility for specific solutes, thereby predicting the extraction efficiency of solvents for target compounds [46–48]. As shown in Figure 5, the blue and red regions in the surface charge density diagram of four flavonoids corresponded to the polar regions. The phenolic hydroxyl group and alcohol hydroxyl group in the blue region of flavonoid molecules exhibit HBD ability, while the carbonyl oxygen and hydroxyl oxygen in the red region confer certain HBA ability. Additionally, the presence of two benzene rings and C and H atoms in the pyranose ring contributes to the formation of a nonpolar region within flavonoid molecules [49].

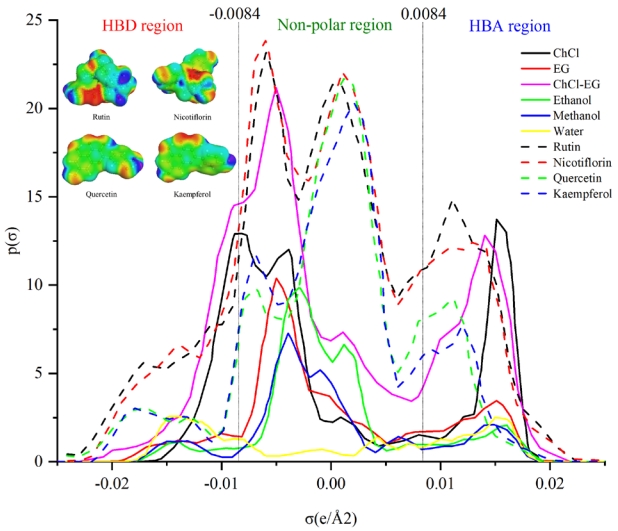

Figure 5. Surface charge density and sigma profiles of different solutions and flavonoids.

Generally, σ-profiles have the capacity to accurately depict the authentic charge distribution and polarity of molecules, as well as to delineate the overall polarization of a molecular surface. These profiles are highly specific to individual molecules, offering a comprehensive portrayal of their unique characteristics. The σ-profile is typically segmented into three distinct regions: The hydrogen bond acceptor (HBA) region ($\sigma > 0.0084$ e/Å^2), the hydrogen bond donor (HBD) region ($\sigma < -0.0084$ e/Å^2), and the non-polar region (-0.0084 e/Å$^2 < \sigma < 0.0084$ e/Å^2) [50]. For extraction, if the target compound and solvent have complementary σ-profiles, they are more likely to exhibit high solubility and extractability [49,51]. Based on the discussion of the σ-profile in Figure 5, the four target flavonoid compounds (rutin, quercetin, kaempferol, and nicotiflorin) in this study are all inclined to be HBAs in the solution; thus, these will have more affinity for the solvent that showed HBD ability when doing the extraction.

Through the optimal NADES screening, the HBA of the optimal NADES was ChCl, and the HBD was EG. It can be seen that ChCl had both HBD (-0.0161 e/Å^2 to -0.0084 e/Å^2) and HBA (0.0084 e/Å^2 to 0.0189 e/Å^2) regions, which indicated that ChCl had both HBA and HBD abilities. The σ-profile of EG was distributed within the range from -0.0188 e/Å^2 to 0.0191 e/Å^2, and the peaks gathering between -0.0811 e/Å^2 and 0.0049 e/Å^2 were high, which was ascribed to the CH_2 groups. In the meantime, the σ-profile extended into the positive polarity region, indicating that EG was predisposed to act as an HBA. For the optimal NADES ChCl-EG, the σ-profile extended widely into a positive polarity region of 0.0212 e/Å^2 and a negative polarity region of -0.0223 e/Å^2, which meant it could possibly interact with both HBD and HBA.

Focusing on traditional solvents, methanol and ethanol both exhibited a symmetric curve with a narrow peak primarily distributed within the nonpolar region due to H

and C atoms in the alkyl group, and the regions associated with HBD and HBA caused by the presence of H and O atoms on the -OH group were fairly small. For H_2O, the nonpolar region was relatively small, and the other two polar regions were nearly identical in size, estimating that the HBA and HBD capabilities were very close. The order of HBD region size among several solutions was: ChCl-EG > H_2O > methanol > ethanol. Due to the flavonoid compounds in FTB having strong HBA ability, ChCl-EG was easy to form hydrogen bonds with flavonoid compounds; therefore, it had stronger extraction efficiency than traditional solvents. On the other hand, the non-polar region size of ChCl-EG was much larger than that of traditional solvents. Based on the similarity–intermiscibility theory, a greater nonpolar region within the solvent leads to an increased extraction yield [52].

3.8. Microstructural Analysis of Extraction Residue

In order to better demonstrate the extent of damage to the sample caused by ultrasound-assisted extraction coupled with ChCl-EG, the microstructure of FTB powder was examined before and after extraction utilizing SEM. As shown in Figure 6, the external surface of the FTB powder sample without any treatment was relatively smooth and flat. After ChCl-EG treatment, the surface of the sample appeared rough, and collapse was encountered. This indicates that ChCl-EG has a high penetration and erosion capacity against the cell wall, which allows flavonoids in plant cells to bind to the ChCl-EG solution more easily. Furthermore, ultrasonication in combination with ChCl-EG induced a significant rupture of the outer surface of the sample; more rough surfaces were observed, which is consistent with prior research conducted by Wang et al. and Cao et al. [35,53]. In our study, due to the strong affinity of ChCl-EG towards flavonoids in FTB powder, as well as its high penetration and erosion capabilities on the cell wall, a greater number of intracellular structures were exposed to the ultrasonic environment. Consequently, this led to an increased generation of micro-jets through asymmetric collapse or implosion. This phenomenon can be likened to a miniature pump that effectively expels more intracellular components from the cell while facilitating enhanced solvent infiltration into the cell, thereby significantly improving flavonoid extraction efficiency.

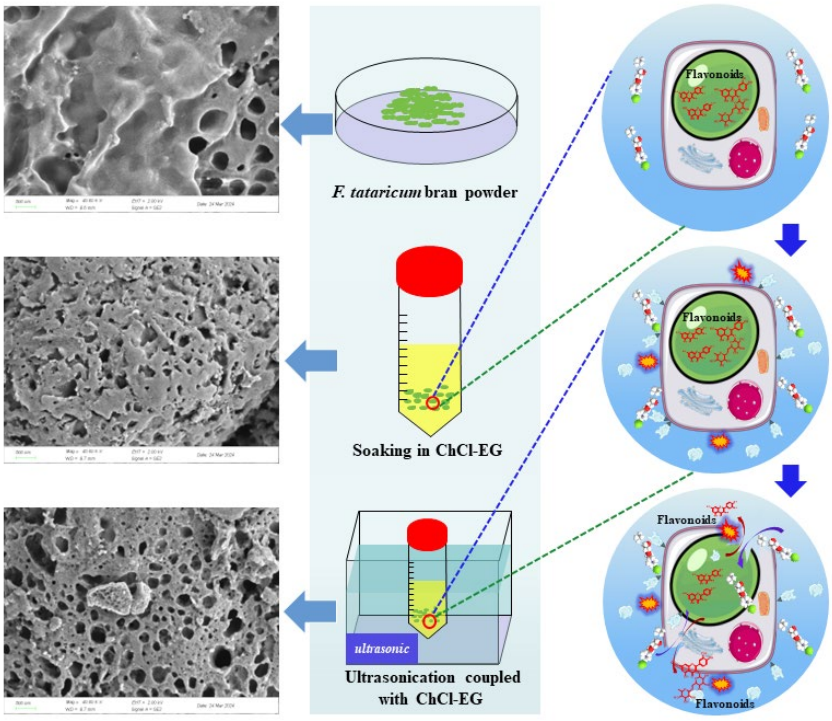

Figure 6. Scanning electron micrographs of FTB before and after extraction with UAE + ChCl-EG.

4. Conclusions

In the present study, eleven kinds of flavonoids were identified from FTB by UPLC-Q-TOF-MS, and HPLC-DAD analysis revealed that four compounds, including rutin, quercetin, kaempferol, and nicotiflorin, were the most significant components. Then, a suitable NADS-UAE method for extracting rutin, quercetin, kaempferol, and nicotiflorin from FTB was successfully established. The best extraction solvent was ChCl-EG, which had the highest total extraction yield for four flavonoids in FTB. After a single-factor experiment and RSM-BBD optimization, the optimal parameters were as follows: Ultrasonic time of 268 s, ultrasonic temperature of 76 °C, and liquid–solid ratio of 43 mL/g. Under this condition, the total flavonoid yield was 40.29 mg/g, which was highly consistent with the predicted value (40.41 mg/g). Afterwards, FT-IR spectra, COSMO model, and microstructural analysis revealed that the formation of hydrogen bonds between ChCl and EG creates a strong polarity and non-polarity region in ChCl-EG, as well as a strong penetration and corrosion ability on the cell wall. Meanwhile, paired with the cavitation effect of ultrasound, NADES-UAE demonstrated high extraction efficiency in the extraction of flavonoids from TFB. In conclusion, NADES-UAE extraction is considered a green, efficient, and sustainable method for FTB flavonoids.

Supplementary Materials: The following supporting information can be downloaded at: https://www.mdpi.com/article/10.3390/separations11050145/s1. Supplementary Material S1: MS spectra of identified flavonoids; Supplementary Material S2: HPLC chromatograms of flavonoids extracted by different solvents.

Author Contributions: Conceptualization, Z.X.; methodology, Z.X., X.D. and J.Q.; formal analysis, Z.X. and S.X.; writing-original draft preparation, Z.X.; writing-review and editing, Z.X. and X.D.; supervision, Z.X. All authors have read and agreed to the published version of the manuscript.

Funding: This research was funded by the Open Project Program of Panxi Crops Research and Utilization Key Laboratory of Sichuan Province (XNFZ2107, SZ22ZZ05) and Doctoral Scientific Research Foundation of Xichang University (YBZ202102).

Institutional Review Board Statement: Not applicable.

Informed Consent Statement: Not applicable.

Data Availability Statement: The dataset generated in this article can be provided to the corresponding author upon request.

Acknowledgments: The authors would like to thank the contribution of Guanfeng Deng from Sichuan agricultural university for his support in operating computer software.

Conflicts of Interest: The authors declare no conflicts of interest.

References

1. Wang, L.; Zhao, J.; Mao, Y.; Liu, L.; Li, C.; Wu, H.; Zhao, H.; Wu, Q. Tartary buckwheat rutin: Accumulation, metabolic pathways, regulation mechanisms, and biofortification strategies. *Plant Physiol. Biochem.* **2024**, *208*, 108503. [CrossRef] [PubMed]
2. Zhu, F. Chemical composition and health effects of Tartary buckwheat. *Food Chem.* **2016**, *203*, 231–245. [CrossRef] [PubMed]
3. Peng, L.X.; Wei, L.J.; Yi, Q.; Chen, G.H.; Yao, Z.D.; Yan, Z.Y.; Zhao, G. In vitro potential of flavonoids from tartary buckwheat on antioxidants activity and starch digestibility. *Int. J. Food Sci. Technol.* **2019**, *54*, 2209–2218. [CrossRef]
4. Zhou, X.-L.; Chen, Z.-D.; Zhou, Y.-M.; Shi, R.-H.; Li, Z.-J. The effect of tartary buckwheat flavonoids in inhibiting the proliferation of MGC80-3 cells during seed germination. *Molecules* **2019**, *24*, 3092. [CrossRef] [PubMed]
5. Zou, L.; Wu, D.; Ren, G.; Hu, Y.; Peng, L.; Zhao, J.; Garcia-Perez, P.; Carpena, M.; Prieto, M.A.; Cao, H.; et al. Bioactive compounds, health benefits, and industrial applications of Tartary buckwheat (*Fagopyrum tataricum*). *Crit. Rev. Food Sci. Nutr.* **2023**, *63*, 657–673. [CrossRef] [PubMed]
6. Ge, R.H.; Wang, H. Nutrient components and bioactive compounds in tartary buckwheat bran and flour as affected by thermal processing. *Int. J. Food Prop.* **2020**, *23*, 127–137. [CrossRef]
7. Aktaş, H.; Kurek, M.A. Deep eutectic solvents for the extraction of polyphenols from food plants. *Food Chem.* **2024**, *444*, 138629. [CrossRef] [PubMed]
8. Saini, A.; Kumar, A.; Panesar, P.S.; Thakur, A. Potential of deep eutectic solvents in the extraction of value-added compounds from agro-industrial by-products. *Appl. Food Res.* **2022**, *2*, 100211. [CrossRef]

9. Socas-Rodríguez, B.; Torres-Cornejo, M.V.; Álvarez-Rivera, G.; Mendiola, J.A. Deep Eutectic Solvents for the Extraction of Bioactive Compounds from Natural Sources and Agricultural By-Products. *Appl. Sci.* **2021**, *11*, 4897. [CrossRef]
10. Benvenutti, L.; Zielinski, A.A.F.; Ferreira, S.R.S. Which is the best food emerging solvent: IL, DES or NADES? *Trends Food Sci. Technol.* **2019**, *90*, 133–146. [CrossRef]
11. Zhang, X.-J.; Liu, Z.-T.; Chen, X.-Q.; Zhang, T.-T.; Zhang, Y. Deep eutectic solvent combined with ultrasound technology: A promising integrated extraction strategy for anthocyanins and polyphenols from blueberry pomace. *Food Chem.* **2023**, *422*, 136224. [CrossRef]
12. Rashid, R.; Mohd Wani, S.; Manzoor, S.; Masoodi, F.A.; Masarat Dar, M. Green extraction of bioactive compounds from apple pomace by ultrasound assisted natural deep eutectic solvent extraction: Optimisation, comparison and bioactivity. *Food Chem.* **2023**, *398*, 133871. [CrossRef] [PubMed]
13. Jeong, K.M.; Zhao, J.; Jin, Y.; Heo, S.R.; Han, S.Y.; Yoo, D.E.; Lee, J. Highly efficient extraction of anthocyanins from grape skin using deep eutectic solvents as green and tunable media. *Arch. Pharmacal Res.* **2015**, *38*, 2143–2152. [CrossRef] [PubMed]
14. Oroian, M.; Ursachi, F.; Dranca, F. Ultrasound-Assisted Extraction of Polyphenols from Crude Pollen. *Antioxidants* **2020**, *9*, 322. [CrossRef] [PubMed]
15. Milićević, N.; Kojić, P.; Sakač, M.; Mišan, A.; Kojić, J.; Perussello, C.; Banjac, V.; Pojić, M.; Tiwari, B. Kinetic modelling of ultrasound-assisted extraction of phenolics from cereal brans. *Ultrason. Sonochem.* **2021**, *79*, 105761. [CrossRef]
16. Zheng, B.; Yuan, Y.; Xiang, J.; Jin, W.; Johnson, J.B.; Li, Z.; Wang, C.; Luo, D. Green extraction of phenolic compounds from foxtail millet bran by ultrasonic-assisted deep eutectic solvent extraction: Optimization, comparison and bioactivities. *LWT* **2022**, *154*, 112740. [CrossRef]
17. Xiang, Z.; Xia, C.; Feng, S.; Chen, T.; Zhou, L.; Liu, L.; Kong, Q.; Yang, H.; Ding, C. Assessment of free and bound phenolics in the flowers and floral organs of two Camellia species flower and their antioxidant activities. *Food Biosci.* **2022**, *49*, 101905. [CrossRef]
18. Huo, J.; Ni, Y.; Li, D.; Qiao, J.; Huang, D.; Sui, X.; Zhang, Y. Comprehensive structural analysis of polyphenols and their enzymatic inhibition activities and antioxidant capacity of black mulberry (*Morus nigra* L.). *Food Chem.* **2023**, *427*, 136605. [CrossRef]
19. Yang, Z.; Shi, L.; Qi, Y.; Xie, C.; Zhao, W.; Barrow, C.J.; Dunshea, F.R.; Suleria, H.A.R. Effect of processing on polyphenols in butternut pumpkin (*Cucurbita moschata*). *Food Biosci.* **2022**, *49*, 101925. [CrossRef]
20. Huang, H.; Ni, Z.-J.; Wu, Z.-F.; Ma, Y.-L.; Hu, F.; Thakur, K.; Zhang, J.-G.; Khan, M.R.; Wei, Z.-J. Comparison of polyphenols in Goji (*Lycium barbarum* L.) leaves at different leaf positions under different extraction methods. *Ind. Crops Prod.* **2024**, *209*, 117982. [CrossRef]
21. Amaya-Cruz, D.M.; Pérez-Ramírez, I.F.; Delgado-García, J.; Mondragón-Jacobo, C.; Dector-Espinoza, A.; Reynoso-Camacho, R. An integral profile of bioactive compounds and functional properties of prickly pear (*Opuntia ficus* indica L.) peel with different tonalities. *Food Chem.* **2019**, *278*, 568–578. [CrossRef] [PubMed]
22. Choi, Y.H.; Spronsen, J.V.; Dai, Y.; Verberne, M.; Hollmann, F.; Arends, I.W.C.E.; Witkamp, G.-J.; Verpoorte, R. Are Natural Deep Eutectic Solvents the Missing Link in Understanding Cellular Metabolism and Physiology? *Plant Physiol.* **2011**, *156*, 1701–1705. [CrossRef] [PubMed]
23. Dai, Y.; Witkamp, G.-J.; Verpoorte, R.; Choi, Y.H. Natural Deep Eutectic Solvents as a New Extraction Media for Phenolic Metabolites in *Carthamus tinctorius* L. *Anal. Chem.* **2013**, *85*, 6272–6278. [CrossRef] [PubMed]
24. Cao, C.; Nian, B.; Li, Y.; Wu, S.; Liu, Y. Multiple Hydrogen-Bonding Interactions Enhance the Solubility of Starch in Natural Deep Eutectic Solvents: Molecule and Macroscopic Scale Insights. *J. Agric. Food. Chem.* **2019**, *67*, 12366. [CrossRef] [PubMed]
25. Cvjetko Bubalo, M.; Ćurko, N.; Tomašević, M.; Kovačević Ganić, K.; Radojčić Redovniković, I. Green extraction of grape skin phenolics by using deep eutectic solvents. *Food Chem.* **2016**, *200*, 159–166. [CrossRef]
26. Ijardar, S.P.; Singh, V.; Gardas, R.L. Revisiting the Physicochemical Properties and Applications of Deep Eutectic Solvents. *Molecules* **2022**, *27*, 1368. [CrossRef]
27. Zainal-Abidin, M.H.; Eng, J.J.; Khairuzi, K.; Kristianto, S.; Asyraf Wan Mahmood, W.M.; Al-Fakih, A.M.; Matmin, J.; Wahab, R.A.; Abdullah, F.; Mohamad, M.F.; et al. Effectiveness of ammonium-based deep eutectic solvents in extracting polyphenol from Chlorella vulgaris. *Algal Res.* **2024**, *79*, 103436. [CrossRef]
28. Mero, A.; Koutsoumpos, S.; Giannios, P.; Stavrakas, I.; Moutzouris, K.; Mezzetta, A.; Guazzelli, L. Comparison of physicochemical and thermal properties of choline chloride and betaine-based deep eutectic solvents: The influence of hydrogen bond acceptor and hydrogen bond donor nature and their molar ratios. *J. Mol. Liq.* **2023**, *377*, 121563. [CrossRef]
29. AlOmar, M.K.; Hayyan, M.; Alsaadi, M.A.; Akib, S.; Hayyan, A.; Hashim, M.A. Glycerol-based deep eutectic solvents: Physical properties. *J. Mol. Liq.* **2016**, *215*, 98–103. [CrossRef]
30. Zhan, A.; Niu, D.; Li, K.; Li, J. Characterization of some sucrose-based deep eutectic solvents and their effect on the solubility of piroxicam. *J. Mol. Liq.* **2023**, *377*, 121556. [CrossRef]
31. Rodrigues, L.A.; Cardeira, M.; Leonardo, I.C.; Gaspar, F.B.; Radojčić Redovniković, I.; Duarte, A.R.C.; Paiva, A.; Matias, A.A. Deep eutectic systems from betaine and polyols—Physicochemical and toxicological properties. *J. Mol. Liq.* **2021**, *335*, 116201. [CrossRef]
32. Liu, Y.; Friesen, J.B.; McAlpine, J.B.; Lankin, D.C.; Chen, S.-N.; Pauli, G.F. Natural Deep Eutectic Solvents: Properties, Applications, and Perspectives. *J. Nat. Prod.* **2018**, *81*, 679–690. [CrossRef]
33. Ke, J.; Ran, B.; Sun, P.; Cheng, Y.; Chen, Q.; Li, H. An Evaluation of the Absolute Content of Flavonoids and the Identification of Their Relationship with the Flavonoid Biosynthesis Genes in Tartary Buckwheat Seeds. *Agronomy* **2023**, *13*, 3006. [CrossRef]

34. Liu, Y.; Zhe, W.; Zhang, R.; Peng, Z.; Wang, Y.; Gao, H.; Guo, Z.; Xiao, J. Ultrasonic-assisted extraction of polyphenolic compounds from *Paederia scandens* (Lour.) Merr. Using deep eutectic solvent: Optimization, identification, and comparison with traditional methods. *Ultrason. Sonochem.* **2022**, *86*, 106005. [CrossRef] [PubMed]
35. Wang, W.; Pan, Y.; Zhao, J.; Wang, Y.; Yao, Q.; Li, S. Development and optimization of green extraction of polyphenols in *Michelia alba* using natural deep eutectic solvents (NADES) and evaluation of bioactivity. *Sustain. Chem. Pharm.* **2024**, *37*, 101425. [CrossRef]
36. Dai, Y.; van Spronsen, J.; Witkamp, G.J.; Verpoorte, R.; Choi, Y.H. Natural deep eutectic solvents as new potential media for green technology. *Anal. Chim. Acta* **2013**, *766*, 61–68. [CrossRef] [PubMed]
37. Cunha, S.C.; Fernandes, J.O. Extraction techniques with deep eutectic solvents. *TrAC Trend. Anal. Chem.* **2018**, *105*, 225–239. [CrossRef]
38. Zhen, S.; Chen, S.; Geng, S.; Zhang, H.; Chen, Y.; Liu, B. Ultrasound-Assisted Natural Deep Eutectic Solvent Extraction and Bioactivities of Flavonoids in *Ampelopsis grossedentata* Leaves. *Foods* **2022**, *11*, 668. [CrossRef] [PubMed]
39. Saha, S.K.; Dey, S.; Chakraborty, R. Effect of choline chloride-oxalic acid based deep eutectic solvent on the ultrasonic assisted extraction of polyphenols from Aegle marmelos. *J. Mol. Liq.* **2019**, *287*, 110956. [CrossRef]
40. Wang, W.; An, M.; Zhao, G.; Wang, Y.; Yang, D.; Zhang, D.; Zhao, L.; Han, J.; Wu, G.; Bo, Y. Ultrasonic-assisted customized natural deep eutectic solvents extraction of polyphenols from Chaenomeles speciosa. *Microchem. J.* **2023**, *193*, 108952. [CrossRef]
41. Dey, S.; Rathod, V.K. Ultrasound assisted extraction of β-carotene from Spirulina platensis. *Ultrason. Sonochem.* **2013**, *20*, 271–276. [CrossRef]
42. Hao, C.; Chen, L.; Dong, H.; Xing, W.; Xue, F.; Cheng, Y. Extraction of Flavonoids from Scutellariae Radix using Ultrasound-Assisted Deep Eutectic Solvents and Evaluation of Their Anti-Inflammatory Activities. *ACS Omega* **2020**, *5*, 23140–23147. [CrossRef]
43. Dzah, C.S.; Duan, Y.; Zhang, H.; Wen, C.; Zhang, J.; Chen, G.; Ma, H. The effects of ultrasound assisted extraction on yield, antioxidant, anticancer and antimicrobial activity of polyphenol extracts: A review. *Food Biosci.* **2020**, *35*, 100547. [CrossRef]
44. Hong, S.M.; Kamaruddin, A.H.; Nadzir, M.M. Sustainable ultrasound-assisted extraction of polyphenols from Cinnamomum cassia bark using hydrophilic natural deep eutectic solvents. *Process Biochem.* **2023**, *132*, 323–336. [CrossRef]
45. Hayyan, M.; Abo-Hamad, A.; AlSaadi, M.A.; Hashim, M.A. Functionalization of graphene using deep eutectic solvents. *Nanoscale Res. Lett.* **2015**, *10*, 1004. [CrossRef] [PubMed]
46. Huang, L.; Guo, Y.; Jin, T.; Yan, K.; Liu, X.; He, S.; Li, L.; Gong, Y.; Ma, J.; Yu, H.; et al. Extraction of triterpene acids from loquat leaves via a novel hydrophobic deep eutectic solvent screened by COSMO-SAC model. *J. Clean. Prod.* **2023**, *427*, 139274. [CrossRef]
47. Oliveira, G.; Wojeicchowski, J.P.; Farias, F.O.; Igarashi-Mafra, L.; de Pelegrini Soares, R.; Mafra, M.R. Enhancement of biomolecules solubility in aqueous media using designer solvents as additives: An experimental and COSMO-based models' approach. *J. Mol. Liq.* **2020**, *318*, 114266. [CrossRef]
48. Wang, D.; Zhang, M.; Law, C.L.; Zhang, L. Natural deep eutectic solvents for the extraction of lentinan from shiitake mushroom: COSMO-RS screening and ANN-GA optimizing conditions. *Food Chem.* **2024**, *430*, 136990. [CrossRef]
49. Cui, Z.; Djocki, A.V.E.; Yao, J.; Wu, Q.; Zhang, D.; Nan, S.; Gao, J.; Li, C. COSMO-SAC-supported evaluation of natural deep eutectic solvents for the extraction of tea polyphenols and process optimization. *J. Mol. Liq.* **2021**, *328*, 115406. [CrossRef]
50. Delley, B. From molecules to solids with the DMol3 approach. *J. Chem. Phys.* **2000**, *113*, 7756–7764. [CrossRef]
51. Lazović, M.; Cvijetić, I.; Jankov, M.; Milojković-Opsenica, D.; Trifković, J.; Ristivojević, P. COSMO-RS in prescreening of Natural Eutectic Solvents for phenolic extraction from *Teucrium chamaedrys*. *J. Mol. Liq.* 2 **2023**, *387*, 122649. [CrossRef]
52. Cheng, H.; Liu, C.; Zhang, J.; Chen, L.; Zhang, B.; Qi, Z. Screening deep eutectic solvents for extractive desulfurization of fuel based on COSMO-RS model. *Chem. Eng. Process.—Process Intensif. Chem. Eng. Process.* **2018**, *125*, 246–252. [CrossRef]
53. Cao, Y.; Song, Z.; Dong, C.; Ni, W.; Xin, K.; Yu, Q.; Han, L. Green ultrasound-assisted natural deep eutectic solvent extraction of phenolic compounds from waste broccoli leaves: Optimization, identification, biological activity, and structural characterization. *LWT* **2023**, *190*, 115407. [CrossRef]